ACS Partner Journal

ACCOUNTS
—of materials research—

pubs.acs.org/amrcda

Article

Hardening Effects in Superhard Transition-Metal Borides

Lisa E. Pangilinan, Shanlin Hu, Spencer G. Hamilton, Sarah H. Tolbert,* and Richard B. Kaner*

Cite This: https://doi.org/10.1021/accountsmr.1c00192

Read Online

ACCESS | Metrics & More | Article Recommendations

CONSPECTUS: Mechanical hardness is a physical property used to gauge the applications of materials in the manufacturing and machining industries. Because of their high hardness and wear resistance, superhard materials (Vickers hardness, $H_v \geq 40$ GPa) are commonly used as cutting tools and abrasives. Although diamond is the hardest known material used for industrial applications, its synthesis requires both high pressure and high temperature. Interest in the field of superhard materials research has led to the search for alternatives with high hardness and thermal stability at low cost. The discovery of novel ultraincompressible, superhard materials has largely developed through trial and error along two paths. In one approach, researchers combine light elements, such as boron, carbon, nitrogen, and oxygen, often at high pressure, to replicate the highly directional, dense, covalent bonds of diamond. In the second approach, these light elements (B, C, N, and O) are combined with highly incompressible, electron-rich transition metals to form dense covalently bonded networks at ambient pressure.

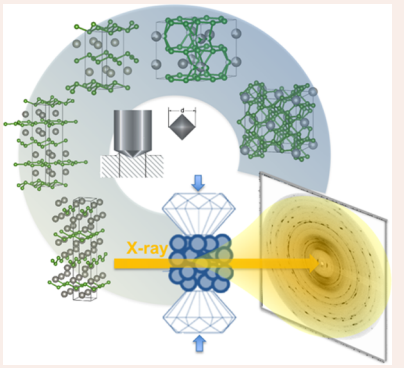

In this Account, we highlight our progress in developing superhard transition-metal borides through solid solution effects and grain boundary strengthening. We begin with a review of the factors that contribute to a material's hardness and guide our design parameters of high electron density and high covalent bond density in the search for new materials. In subsequent sections, we examine various metal boride systems with increasing bond covalency and structural complexity, from metal-rich mono- and diborides to boron-rich tetra- and dodecaborides. The metal borides discussed in this Account are formed at ambient pressure using high-temperature solid-state techniques such as arc melting and molten flux synthesis. By characterizing these materials through both Vickers hardness testing and high-pressure experiments, we gain insight into the coupled effects of bonding and grain morphology on mechanical properties. Finally, we provide an outlook into the expedited discovery and accessible compositions for future materials. We hope that the materials and methods discussed in this Account offer new opportunities for the design and synthesis of the next generation of superhard materials for industrial applications.

1. INTRODUCTION

From rocks to metals and ceramics, hardness is a property used to evaluate a material's resistance to deformation (i.e., scratching or imprinting). For instance, the Mohs scale is a qualitative method of comparing hardness through scratch resistance. Materials are ranked on the basis of their ability to scratch another material, with hardness values ranging from 1 (soft materials such as talc) to 10 (diamond). Because of its lack of precision, the Mohs scale does not gauge the performance of hard materials in an industrial setting. To quantify hardness, an indenter is pressed against the surface of a sample at a constant applied load. The size of the indent is then correlated with a hardness value, and indenters of different shapes produce different values. For example, in the Vickers microindentation test, the hardness is quantified by the average diagonal length of the impression made by a regular pyramidal indenter at a constant applied force. Materials that exceed a threshold Vickers hardness value ($H_v \geq 40$ GPa) are classified as superhard.

The applications of hard materials are most evident in the manufacturing and machining industries, where these materials are used to cut or grind softer materials. Currently, diamond, cubic boron nitride, and tungsten carbide are the most commercially relevant hard materials. Although diamond is the hardest known material (H_v = 115 GPa at a load of 4.9 N for synthetic single-crystal diamond),[1] it graphitizes at high temperature and reacts with iron to form brittle carbides when used to machine ferrous materials. The alternative, cubic boron nitride (*c*-BN), is insoluble in iron but has approximately half the hardness of diamond (H_v = 62 GPa at 4.9 N for single-crystal *c*-BN).[2] In addition, both materials require high-pressure, high-temperature (HPHT) conditions to form and are therefore expensive. Tungsten carbide (WC) can be used, but it is much softer (H_v = 23 GPa) than diamond and *c*-BN.[3,4] These limitations motivate the search for new

Received: September 1, 2021
Revised: November 30, 2021

Table 1. Oxidation Resistance and Hardness Values for Selected Materials[a]

parent crystal structure	synthesis ratio	Hv at 4.9 N (GPa)	Hv at 0.49 N (GPa)	oxidation resistance (°C)	ref
WB	W0.5Ta0.5:1.0B	~22.9	42.8 ± 2.6	550	18
WB_2	W: 2.1B	21.9 ± 1.3	29.5 ± 1.7	520	19
	W0.94Nb0.06:2.1B	25.5 ± 1.3	40.3 ± 1.6	550	
	W0.92Ta0.08:2.1 B	25.2 ± 1.4	41.0 ± 1.2	570	
ReB_2	Re: 2.2SB	29.31 ± 0.77	40.45 ± 2.79	~500	20
	Re0.52W0.48:2.25B	30.92 ± 0.92	47.2 ± 1.06		
WB_4	W: 12B	28.1 ± 1.4	43.3 ± 2.9	400	21
	W0.94Ta0.02:12B	33.5 ± 0.3	52.8 ± 0.6		22
	W0.96Mn0.04:12B	31.7 ± 0.2	53.7 ± 0.5		
	W0.9Mn0.1B: 12B	31.4 ± 0.3	53.9 ± 0.5		
	W0.9Cr0.1:12B	32.4 ± 0.4	53.5 ± 0.5		
	W0.94Ta0.02Mn0.04:12B	30.9 ± 0.2	55.8 ± 0.5		
	W0.93Ta0.02Cr0.05:12B	31.7 ± 0.2	57.3 ± 0.5	420	
	W0.92Ti0.08:12B	~32.0	50.9 ± 2.2	460	23
	W0.92Zr0.08:12B	34.7 ± 0.65	55.9 ± 2.7	510	
	W0.94Hf0.06:12B	~32.1	51.6 ± 2.8	490	
	W0.94Y0.06:11.6B	~31.0	50.2 ± 2.4	470	24
	W0.92Sc0.08:11.6B	~32.1	48.9 ± 2.5	525	
	W0.96Gd0.04:11.6B	~29.5	48.0 ± 2.1	465	
	W0.94Tb0.06:11.6B	~30.8	46.3 ± 2.6		
	W0.94Dy0.06:11.6B	~31.2	48.5 ± 2.3		
	W0.92Ho0.08:11.6B	~29.5	46.5 ± 2.4		
	W0.94Er0.06:11.6B	~28.8	47.2 ± 2.9		
MB_{12}	Y: 20B	28.5 ± 0.7	41.6 ± 1.3	715	25, 26
	1.0Zr: 20B	29.6 ± 0.7	41.3 ± 1.1	610	
	Y0.5Hf0.5:20B	~31.1	45 ± 1.9		27
	Zr0.50Y0.25Gd0.25:20B	28.7 ± 1.3	46.9 ± 2.4		26

[a]Hardness measurements without error values were estimated from experimental data from each corresponding reference.

superhard materials that can bridge the gap between diamond and relatively softer materials such as WC. Thus, the focus of superhard materials research is to create materials with high hardness, enhanced chemical stability, and a low cost of production.

All known superhard materials exhibit high bulk moduli (i.e., incompressibility). However, having high incompressibility does not necessarily result in a superhard material.[5] Although diamond (K_0 = 438−446 GPa)[6] and osmium (K_0 = 395−462 GPa)[7,8] are both ultraincompressible, diamond is significantly harder than osmium (H_v = 115 vs 4 GPa, respectively).[1,9] The hardness is directly related to the resistance to plane slippage and dislocation motion. Diamond's highly covalent bonding network contributes to its great resistance to dislocation movement and extreme hardness, whereas Os, containing weak metallic bonding, is much more susceptible to slip.

Inspired by the highly covalent bonding network found in diamond, our group has focused its efforts on designing new superhard materials by combining incompressible transition-metal atoms with light elements (e.g., boron and carbon).[10] We began our investigation with osmium diboride (OsB_2), an Os metal lattice with boron sheets in a boatlike configuration.[11] Although OsB_2 is not superhard, the addition of boron to the Os lattice greatly increases its corresponding hardness from 4 to 27 GPa (at 0.49 N).[12] Since our introductory work on OsB_2, we have produced a range of superhard transition-metal borides with the aforementioned design parameters, including ReB_2, WB_4, and MB_{12} and their solid solutions.

Through the combined efforts of Vickers microindentation and high-pressure studies, we have obtained both direct hardness measurements and lattice-specific insight into various superhard materials. To provide a basis for comparison, we list hardness values with the corresponding applied load whenever possible. The concept and measurement techniques of hardness and high-pressure behavior are discussed in a separate book chapter.[13] The scope of this Account is to highlight progress on metal boride systems, outline the factors that contribute to their high hardness, and indicate future avenues in the field of superhard materials research.

2. COMBINING HARDNESS MEASUREMENTS WITH HIGH-PRESSURE STUDIES

Hardness is a mechanical property that results from both intrinsic and extrinsic effects and depends on the chemical bond strength and energy dissipation at grain boundaries, respectively.[10,14] Materials that are intrinsically hard (e.g., diamond and *c*-BN) possess high resistance to both volume and shape changes (bulk modulus and shear modulus, respectively). One method to increase the intrinsic hardness of a material is through solid solution formation, where one type of atom is substituted for another atom. The formation of such solid solutions follows a set of guidelines known as the Hume−Rothery rules, which require the solute and solvent atoms to adopt similar crystal structures, atomic size (<15% difference in atomic radii), electronegativity, and valence electron counts.[15] At the other end of the spectrum, extrinsic effects (e.g., Hall-Petch hardening) can be introduced by creating smaller grains and more grain boundaries in a material.[16] Both solid solution effects and grain boundary hardening impede the dislocation motion by introducing

https://doi.org/10.1021/accountsmr.1c00192
Acc. Mater. Res. XXXX, XXX, XXX−XXX

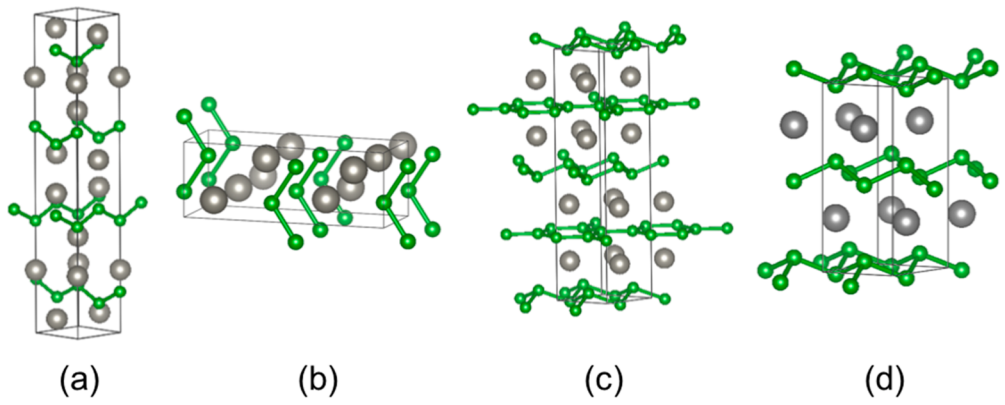

Figure 1. Crystal structures of (a) tetragonal α-WB, (b) orthorhombic β-WB, (c) WB_2, and (d) ReB_2. Gray atoms represent metals, while smaller, green atoms represent boron.

nonuniformity into the crystal lattice, consequently leading to higher hardness.

Although hardness is well quantified as an indentation value, the value itself does not provide insight into the chemical bonding and mechanisms for mechanical failure. In situ high-pressure radial diffraction, however, allows us to directly study the lattice-specific mechanisms for intrinsic hardening. When a material is under uniaxial compression, the lattice planes undergo deformation. The shift of the corresponding d spacings between the high-stress and the low-stress directions is referred to as the differential strain and is given by the ratio between the differential stress (t) and the shear modulus (G) (t/G). Differential strain reveals the degree to which each lattice plane deforms, while differential stress indicates the actual stress each lattice plane sustains during deformation. At the maximum stress, the yield point indicates the onset of plastic deformation, and the corresponding value is defined as the yield strength, which is the maximum stress that the material can sustain before bond breakage. In general, superhard materials possess high yield strength or withstand higher stress before plastic deformation.

3. EXPLORING SUPERHARD TRANSITION-METAL BORIDES

Transition-metal borides possess rich crystal chemistry, with covalent boron arrangements ranging from 1-D chains to 2-D sheets and 3-D networks.[17] The diversity of these crystal structures results in a wide range of metal boride properties (e.g., mechanical, magnetic, and catalytic behavior) and applications. Modifying the complex bonding motifs between metal and boron atoms within the structure results in greater control of material properties. These compounds can be classified by their metal-to-boron atomic ratio (M/B), which generally ranges from >1:4 for metal-rich compounds (also known as low borides) to ≤1:4 for boron-rich compounds (or higher borides).

In this section, we detail studies performed by our group exploring transition-metal boride systems with increasing bond covalency and structural complexity, from metal-rich mono- and diborides to boron-rich tetra- and dodecaborides. Both intrinsic and extrinsic effects are examined to assess the contributions of different hardening mechanisms on bulk and nanomaterials. Material properties for selected metal boride compositions are listed in Table 1. All samples were synthesized via resistive arc-melting of the pure elements unless otherwise stated. Note that Vicker's hardness, determined from the size of the indent under a specific load, is a direct measurement of hardness, which is a combination of intrinsic (i.e., covalency of the crystal structure) and extrinsic (i.e., grain boundary) hardness. As shown in Table 1, the Vicker's hardness at low load (0.49 N) is listed since this is a good indication of usefulness for real world applications, such as cutting and polishing, most of which is done under low load.

3.1. Metal-Rich Borides and Their Derivatives (M/B > 1:4)

Most transition metals form metal-rich borides. These structural types consist of boron atom arrangements that are isolated (e.g., Cr_4B), paired (e.g., $LaCo_2B_2$), single chains (e.g., CrB), double chains (e.g., Ta_3B_4) or sheets (e.g., AlB_2). Many borides in this classification group exhibit notable material properties, such as superconductivity (MgB_2), high hardness, ultraincompressibility (ReB_2, $RhB_{1.1}$, and $IrB_{1.1}$),[28,29] and high melting temperatures for use under extreme conditions (ZrB_2 and HfB_2). Our introductory work in the field of superhard materials began with investigations into lower borides, where lattice expansion is minimized upon incorporating boron atoms into the parent metal crystal structure. Figure 1 shows the crystal structures for metal-rich borides previously investigated in our group. Although most lower borides are not intrinsically superhard, our studies on these systems demonstrate the significant hardness enhancement that can result as solid solution formation suppresses slip in lattice-specific planes.

3.1.1. Tungsten Monoboride (WB). Tungsten monoboride (WB) is a lower boride of tungsten that crystallizes in one of two distinct phases: low temperature (LT) tetragonal α-WB or high-temperature (HT) orthorhombic β-WB (Figure 1a,b). Both phases form bilayers of W atoms but differ in their boron chains, which alternate orthogonally in α-WB and align along the a axis in β-WB. The hardness of WB (H_v = 36.3 GPa at 0.49 N) is limited by the tungsten bilayer slip plane. Tantalum (Ta) has a slightly larger atomic radius than W and similar valency and electronegativity. Ta and W also form the same body-centered cubic structure, thereby satisfying the Hume−Rothery rules of solid solution formation. Moreover, TaB crystallizes into the same orthorhombic boride structure as HT β-WB, resulting in a high degree of Ta solubility in the β-WB structure. By substituting W with increasing amounts of Ta in W sites, the overall hardness increased to a maximum value of 42.8 ± 2.6 GPa at 0.49 N for 50 atomic percentage (at. %) Ta in $W_{0.50}Ta_{0.50}B$.[18] The absence of a secondary phase, demonstrated through XRD and EDS, indicates that increased

https://doi.org/10.1021/accountsmr.1c00192
Acc. Mater. Res. XXXX, XXX, XXX−XXX

hardness in $W_{1-x}Ta_xB$ was achieved through solid solution effects.

High-pressure radial diffraction measurements of $W_{1-x}Ta_xB$ help to explain the increased hardness.[30] As shown in the inset (Figure 2), the (200) and (002) set of planes of $W_{1-x}Ta_xB$

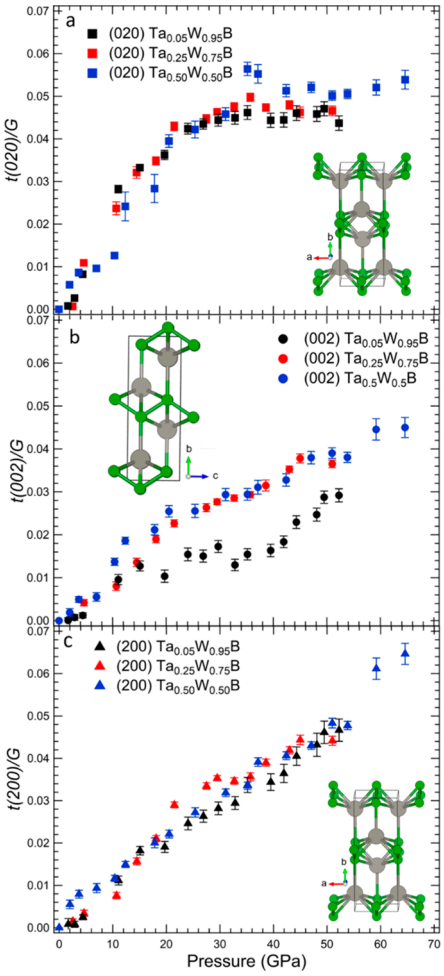

Figure 2. Differential strain in (a) (020), (b) (002), and (c) (200) lattice planes for WB solid solutions with Ta concentrations of 5, 25, and 50%. The insets show the crystal structure of orthorhombic WB with boron atoms in green and tungsten atoms in gray. Adapted with permission from ref 30. Copyright 2019 *J. Appl. Phys.*

intersect the boron−boron chains and bonds, respectively, while the (020) planes cut through the tungsten bilayer. At low Ta content, the (002) plane is much weaker than the (200) or (020) plane, and it shows failure, as evidenced by a plateau in the t/G value (Figure 2b) at relatively modest pressures (~15 GPa). By contrast, the (020) plane in low-Ta materials does not slip until about 25 GPa (Figure 2a), and the (200) plane (Figure 2c) does not slip at experimentally accessible pressures. Upon increasing Ta addition, two things occur. In the first place, the (002) plane is dramatically strengthened so that it is no longer the lowest-pressure failure point in the system. In parallel, both the failure pressure and the failure strain of the (020) plane increase, likely a direct result of the mixed-metal composition in the metal bilayers. In the WB_4 and MB_{12} systems, high hardness is correlated with the covalent boron framework (section 3.2). In contrast, the unique behavior of $W_{1-x}Ta_xB$ suggests that even in the absence of a full boron network, strengthening the weakest lattice planes through solid solution effects is a viable method to develop new superhard materials.

$W_{0.5}Ta_{0.5}B$ nanowires were then synthesized using an aluminum flux at ambient pressure.[31] The aspect ratio of the resultant nanowires was controlled by the concentration of monoboride in the molten flux. A low flux to boride loading ratio led to higher nucleation density and smaller nanocrystals, whereas a high flux to boride ratio resulted in lower density and larger crystallites. These results demonstrate the ability to control the growth and morphology of hard metal borides on the nanoscale.

3.1.2. Tungsten Diboride (WB_2). The crystal structure of tungsten diboride (WB_2) contains alternating flat and corrugated boron sheets between metal layers (Figure 1c). Although WB_2 is not superhard due to easy slip along the flat boron sheets (H_v = 29.5 ± 1.7 GPa at 0.49 N), the material can be hardened by forming solid solutions with metal substitution. For instance, the addition of niobium (Nb) and tantalum (Ta) to the WB_2 structure achieved low load (0.49 N) hardness values of 40.3 ± 1.6 for $W_{0.94}Nb_{0.06}B_2$ and 41.0 ± 1.2 GPa for $W_{0.92}Ta_{0.08}B_2$, which place them in the superhard regime.[19] As a hybrid structure between the common AlB_2 lattice and superhard ReB_2, WB_2 has remained largely overlooked for potential hardness enhancement. However, studies of the formation of solid solutions with WB_2 indicate that even small amounts of metal substitution may lead to greater hardness and oxidation resistance.

3.1.3. Rhenium Diboride (ReB_2). Rhenium diboride is a structure that contains alternating puckered boron sheets and Re layers (Figure 1d). The unique layered structure of ReB_2 results in great resistance to lattice dislocation motion and high Vickers hardness, making ReB_2 the first transition-metal boride studied by our group to be measured in the superhard regime.[28] By doping W into the ReB_2 structure, the Vickers hardness increased from 40.45 ± 2.79 GPa in pure ReB_2 to 47.20 ± 1.06 GPa in $Re_{0.52}W_{0.48}B_2$ under low load (0.49 N).[20] The enhanced Vickers hardness is supported by the improved differential stress in $Re_{0.52}W_{0.48}B_2$, as shown in Figure 3.[14] A series of other ReB_2 solid solutions were made, and both $YRe_{0.5}Cr_{0.5}$: 4B and YScRe: 6B exhibit superhardness.[32]

Further investigation of the combination effects of intrinsic and extrinsic hardening was conducted on nanocrystalline $Re_{0.52}W_{0.48}B_2$ (noted as $ReWB_2$) synthesized through a molten salt method.[14] Although bulk polycrystalline material is usually synthesized via arc melting under high temperature, nanomaterials can be formed through a solution-precipitation mechanism in which the molten salt serves as the solvent and crystalline material forms as a precipitate upon cooling. Since arc-melting heats and cools samples very quickly, it produces large particles (>1 μm) without precise control over grain size. On the other hand, the molten salt method is relatively slow but can produce nanoparticles with tunable crystalline sizes. The formation of nano-$ReWB_2$ through the molten salt method resulted in a significant increase in differential stress compared to bulk $ReWB_2$. In addition, changes in texture, or preferred grain orientation, could be followed in nanocrystalline $ReWB_2$ because of the high quality of the nanocrystal diffraction patterns at high pressure (Figure 4). The texture was plotted in an inverse pole figure, directly mapping the accessible slip systems as functions of pressure, composition, and domain size. The texture intensity is measured in multiples of the mean random distribution

https://doi.org/10.1021/accountsmr.1c00192
Acc. Mater. Res. XXXX, XXX, XXX−XXX

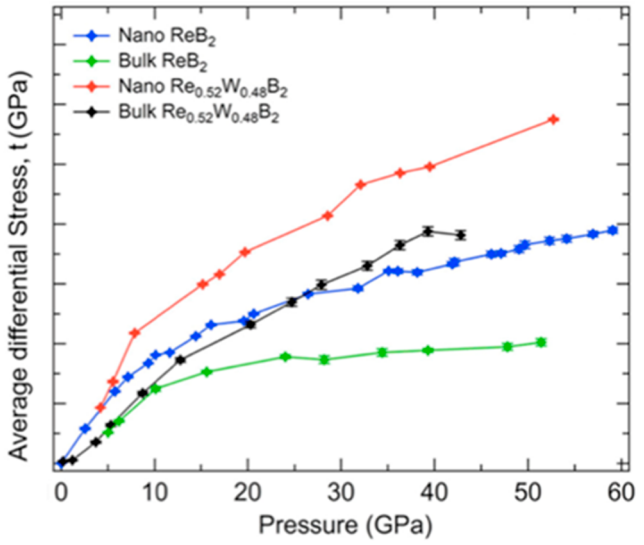

Figure 3. Average differential stress over all observed lattice planes of nano and bulk ReB_2 and $ReWB_2$ as a function of pressure. Adapted with permission from ref 14. Copyright 2019 American Chemical Society.

(m.r.d.), with random texture at 1 and stronger texture at higher values. For both samples, the texture intensity is concentrated at the (0001) corner, indicating that slip predominantly occurs along the boron sheet. In nano-ReB_2, additional slip systems become accessible at higher pressures; however, in nano-$ReWB_2$, solid-solution formation appears to suppress the formation of any additional slip systems. These experiments thus provide direct information about slip under load in superhard metal borides and demonstrate how the combination of size and solid-solution effects can be used to design improved superhard materials.

3.2. Boron-Rich Borides and Their Derivatives (M/B ≤ 1:4)

As the amount of boron relative to the metal increases, the arrangement of boron begins to play an even more important role in the properties of the compound. Tungsten tetraboride (WB_4), for instance, consists of boron sheets with additional boron atoms sitting in partially occupied tungsten sites to create distorted cuboctohedral boron cages[33] (Figure 5a). This

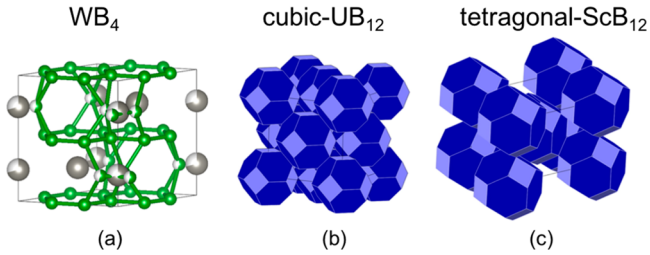

Figure 5. (a) Crystal structure of WB_4, where boron atoms are shown in green and tungsten atoms are represented in gray. Partially occupied sites are shown as partially filled atoms. Polyhedra models of (b) cubic-UB_{12} and (c) tetragonal-ScB_{12} structural-type metal dodecaborides. Adapted with permission from ref 33. Copyright 2016 American Chemical Society.

3-D network of rigid boron−boron bonds is responsible for binding the sheets together and decreasing the anisotropy of the material.[34] This structural motif of cage-like boron frameworks is extended in even higher boride systems such as metal dodecaborides (MB_{12}), which feature boron cuboctahedra surrounding each metal atom in either a face-centered cubic (cubic-UB_{12}, Figure 5b) or body-centered

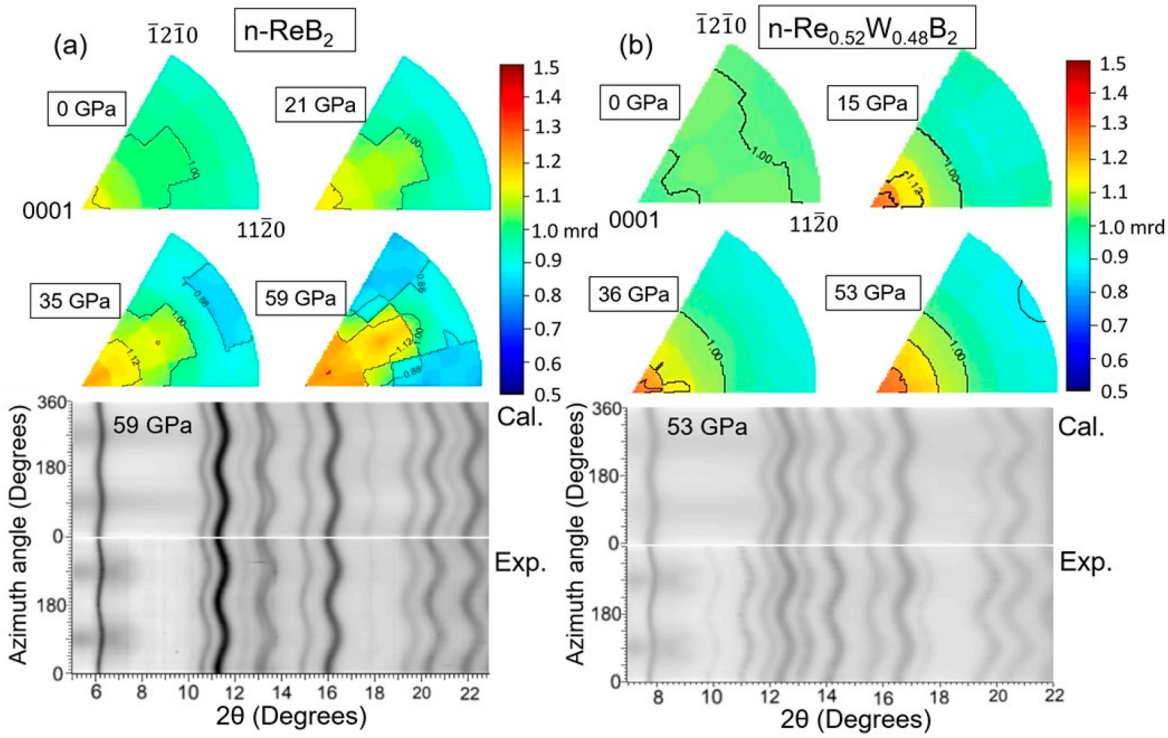

Figure 4. Inverse pole figures for nano-ReB_2 and nano-$ReWB_2$, showing texture evolution with pressure. Adapted with permission from ref 14. Copyright 2019 American Chemical Society.

https://doi.org/10.1021/accountsmr.1c00192
Acc. Mater. Res. XXXX, XXX, XXX−XXX

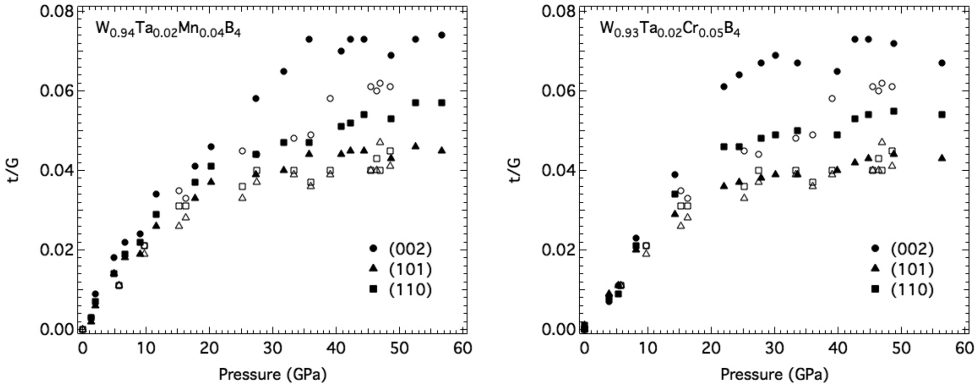

Figure 6. Differential strain of the two hardest ternary solid solutions, $W_{0.94}Ta_{0.02}Mn_{0.04}B_4$ and $W_{0.93}Ta_{0.02}Cr_{0.05}B_4$. In both cases, solid symbols indicate solid solution data, while open symbols correspond to pure WB_4. Adapted with permission from ref22. Copyright 2015 AIP Publishing.

tetragonal (tetragonal-ScB_{12}) arrangement (Figure 5c). These isotropic, 3-D lattice structures of boron-rich borides mimic the crystal structure of diamond and allow relatively malleable metals to cross into the superhard regime.

3.2.1. Tungsten Tetraboride (WB_4). The highest tungsten boride, WB_4, exhibits high hardness (H_v = 43.3 ± 2.9 GPa under 0.49 N) due to a combination of the pseudocage structure formed from the alternating hexagonal layers of boron and boron trimers sitting in the partially occupied tungsten sites (Figure 5a) and its high electron density, resulting from the high metal content. In addition to this highly covalent bonding network, the partially occupied sites can accommodate both substitutional and interstitial dopant atoms. WB_4 solid solutions exhibit enhanced hardness from pure WB_4 due to the atomic size mismatch and changes in valence electron count from doping. In both WB_4 and its solid solutions, the (002) planes, parallel to the boron layers and tungsten atoms, exhibit the greatest resistance to slip, a result that stands in sharp contrast to data on ReB_2 and related compounds, where the (002) planes were uniformly the primary slip systems. The change indicates strengthened cross-linking between boron layers by the formation of the rigid pseudocage structures. For instance, $W_{0.98}Ta_{0.02}B_4$ and $W_{0.9}Cr_{0.1}B_4$ both show a slight increase in differential strain in the (002) plane, while $W_{0.96}Mn_{0.04}B_4$ shows a significant enhancement in differential strain in all lattice planes.[22] The enhanced resistance to shear is confirmed by computational simulations that demonstrate that Cr and Mn doping strengthen the interlayer bonding (B_{hex}–$B_{cluster}$) and Ta doping enhances boron–metal bonding ($B_{cluster}$–M).[35] Extending the binary solid solutions to ternary metal combinations, both $W_{0.94}Ta_{0.02}Mn_{0.04}B_4$ and $W_{0.93}Ta_{0.02}Cr_{0.05}B_4$ show even higher differential strain in all lattice planes compared to the binary WB_4 solid solutions (Figure 6).[22] Furthermore, doping transition metals into the WB_4 structure not only enhances the hardness but in the case of Ta can also stabilize the WB_4 phase with less boron required for synthesis, thereby reducing the overall cost of WB_4 production.[36]

Tuning the composition of WB_4 alloys is also an effective route to altering the grain morphology of WB_4 and thus studying its extrinsic effects on bulk mechanical and thermal properties. Extrinsic hardening was observed in WB_4 solid solutions with group 4 transition metals (Ti, Zr, and Hf).[23] $W_{0.92}Zr_{0.08}B_4$, in particular, developed nanostructured grain morphology, resulting in the highest Vickers hardness of 55.9 ± 2.7 GPa under an applied load of 0.49 N. In comparison to pure WB_4, Y-, Gd-, Tb-, Dy-, Ho-, and Er-doped WB_4 alloys led to "dendritic" grain patterning and enhanced hardness. Moreover, the alloys of WB_4 with Y, Sc, and Gd addition showed improved oxidation resistance.[24]

3.2.2. Metal Dodecaborides (MB_{12}). Metal dodecaborides (MB_{12}) are a class of boron-rich compounds that crystallize into one of two structures containing cuboctahedron cages of 24 boron atoms surrounding a 12-coordinate metal (Figure 5b). Most MB_{12} structures have the cuboctahedra organized in a face-centered cubic arrangement, known as the cubic-UB_{12} structure, but some dodecaborides such as ScB_{12} have the cages organized in a body-centered tetragonal structure, forming the tetragonal-ScB_{12} structure (Figure 5c). Unlike lower boride structures, the hardness of dodecaborides comes from the 3-D symmetric framework of boron cuboctahedra which contain short boron–boron bonds and stiff metal–boron bonds that demonstrate remarkably low anisotropy.[37] In addition, the high boron content of MB_{12} structures such as YB_{12} results in enhanced oxidation resistance (715 °C)[25] when compared to standard cutting materials such as WC (~400 °C).[38] Additionally, metal dodecaborides have low densities (e.g., the density of YB_{12} = 3.44 g/cm^3),[39] which are comparable to that of diamond (3.52 g/cm^3). The superhardness, high oxidative resistance, and low density make metal dodecaborides very promising materials for industrial applications such as machining and protective coatings.

To accommodate the formation of the cuboctahedral cages, there is a restriction on the size of metal atoms that can form a stable MB_{12} structure. Only metals with radii of between 1.603 and 1.801 Å,[40] the radii of zirconium and yttrium, respectively, can form a dodecaboride phase that is stable at ambient pressures. The dodecaboride lattice parameter must fall between 7.408 and 7.500 Å, the values for ZrB_{12} and YB_{12}, respectively. Even slight deviations from this range, such as in hafnium (7.377 Å for HfB_{12})[40] and gadolinium (7.524 Å for GdB_{12}),[40] result in unstable phases. However, stable metal dodecaborides of Hf and Gd can be formed under high pressure (6.5 GPa)[40] or as a solid solution with another stable dodecaboride phase, such as in $Y_{1-x}Hf_xB_{12}$ or $Zr_{1-x}Gd_xB_{12}$.[41] The latter method has the added advantage of solid-solution hardening effects, which increased the Vickers hardness of $Y_{0.5}Hf_{0.5}B_{12}$ to 45.0 ± 1.9 GPa under an applied load of 0.49 N, compared to 40.9 ± 1.6 GPa for the YB_{12} parent compound.[27] These solid-solution systems were then extended to include a range of ternary dodecaborides containing combinations of Zr,

https://doi.org/10.1021/accountsmr.1c00192
Acc. Mater. Res. XXXX, XXX, XXX–XXX

Y, Hf, and Gd.[26] The dodecaboride samples were prepared with excess boron at a nominal metal-to-boron ratio of 1:20. The hardest of these compositions, $Zr_{0.5}Y_{0.25}Gd_{0.25}$:20 B, had a Vickers hardness of 46.9 ± 2.4 GPa compared to 41.3 ± 1.1 and 41.6 ± 1.3 GPa for the 1.0 Zr:20 B and 1.0 Y:20 B compositions, respectively, again both at a 0.49 N applied load. Although the list of metals that can form stable MB_{12} compositions is small, the possibility for binary and ternary solid solutions that can stabilize metals such as Hf and Gd substantially increases the number of conceivable dodecaboride compositions with favorable mechanical and thermal properties for potential use in industrial applications.

4. FUTURE OUTLOOK

4.1. Developing Hard Materials for High-Temperature Applications

Superhard materials capable of operating in oxidizing environments and at high temperatures are desirable for applications in the manufacturing and aerospace industries. For instance, cutting tool materials undergo enormous amounts of force and generate significant heat during cutting or grinding processes, leading to overall tool wear and degradation with increasing temperature.[42] There is a demand for superhard materials that maintain high hardness, chemical stability, and oxidation resistance at elevated temperatures.

Several borides, such as ZrB_2, HfB_2, and TiB_2, are classified as ultra-high-temperature ceramics (UHTCs). These materials have melting temperatures above 3000 °C and have been explored for use in extreme heating environments.[43] ZrB_2 and HfB_2 have been found to be the most oxidation-resistant.[44] However, while these materials experience high oxidation resistance, their hardness decreases with increasing temperature. For example, the Vickers hardness of ZrB_2 decreases from 29.4 GPa at room temperature to ∼9 GPa at 600 °C, while the hardness of HfB_2 decreases from 31.5 to ∼16 GPa at 500 °C.[45] All indentations were made at a load of 0.49 N. Understanding the composition−structure−property relationships of hard materials and their oxidation behavior is vital for creating new materials with desirable properties for industrial applications. Recently, computational studies on understanding the temperature dependence of structural and mechanical properties have provided insights into design rules for novel UHTCs.[46,47] Future areas of research include developing novel materials that optimize high-temperature hardness and oxidation resistance.

4.2. Formation of High-Entropy Borides

Extending from the solid solutions, entropy stabilization was demonstrated in five-component oxides in 2015. Such systems, consisting of five elements in relatively equal concentrations, are defined as high-entropy materials.[48] In a high-entropy system, with an increasing number of elements, the entropic contribution to the total free energy overcomes the enthalpic contribution to drive the formation of a homogeneous single phase. High-entropy materials have since expanded to borides, carbides, nitrides, sulfides, and silicides. Much attention has been focused on synthesizing high-entropy borides with a high density, low-oxygen impurity and refined microstructure through spark plasma sintering (SPS) and the boro/carbothermal reduction of metal oxides. In 2016, Luo et al. first proposed the synthesis of a series of high-entropy diborides by high-energy ball milling followed by SPS and demonstrated enhanced performance in hardness and oxidation resistance.[49] In 2020, Feng et al. proposed a two-step synthesis consisting of boro/carbothermal reduction followed by solid solution formation to produce nanosized phase-pure high-entropy diboride powder.[50] They reported the densification of the high-entropy diboride powder of high purity and fine particle size by SPS and performed Vickers hardness tests on the densified materials.[51] Recently, Chu et al. synthesized nanocrystalline high-entropy diborides and carbides through a high-pressure sintering method and demonstrated excellent mechanical properties.[52,53] A majority of the high-entropy borides that were reported form diborides, typically adopting the AlB_2 structure with alternating boron sheets and high-entropy cation layers. Although high-entropy diborides in general have not reached the Vickers hardness of superhard materials (with the exception of $CrHfTaTiZrB_2$ and $HfTaTiWZrB_2$[54]), these works open a new research area on high-entropy borides that show relatively high hardness with great stability and resilience across applications.[48]

4.3. Discovering New Materials via Machine Learning

High-throughput screening of data using machine learning (ML) has become an integral piece for materials discovery in areas ranging from clean energy and energy transmission to transportation and electronics. Recently, data-driven discovery has been used to more rapidly discover new compositions for superhard materials. Although the extrinsic properties of superhard materials (e.g., morphology and grain size) can be analyzed via simple trial-and-error experimental methods, intrinsic properties of superhard materials, such as electron configurations, atomic radii, and chemical bond strength, are difficult to study in a cooperative, systematic fashion. ML methods have delivered promising results in the field of data-driven discovery for superhard material composites. Brgoch et al. have developed algorithms with support-vector machine regression models that predict superhard alloy compositions based on previous intrinsic experimental data.[55] Specifically, they experimentally synthesized two compounds whose compositions were predicted to be superhard via nonlinear functions that fit closely to training data sourced from literature superhard values. Two compounds, $Mo_{0.9}W_{1.1}BC$ and $ReWC_{0.8}$, were predicted, synthesized, and found to produce hardness values within 10% of the hardness predicted by the ML model. The group has also recently published findings on load-dependent predictions for Vickers hardness based only on chemical composition by using training models with existing sparse data sets, a common issue found when searching for training data from the published literature.[56] This level of predictive power could allow for the hardness of materials at various loads to be extrapolated if only one load is reported. Using ensemble learning designed to rule out hypotheses outliers after multiple training runs, algorithms achieving high accuracy (R^2 = 0.97) were created and 68 superhard materials were discovered from a set of 66 000 compounds in Pearson's crystal data set, a reasonable value because these materials are scarce. These compounds include derivatives of already-reported superhard materials and previously unknown superhard materials, such as ScB_2C_2 and $Sc_3B_{51}C_{0.75}$.[56] This new ensemble machine learning method has demonstrated excellent quantitative agreement with reported values for *c*-BN, ReB_2, and WB_4 (Figure 7).

Although the search for new superhard materials can benefit greatly from automated discovery, it is still a tool, rather than a replacement, for the entire composition selection process.

https://doi.org/10.1021/accountsmr.1c00192
Acc. Mater. Res. XXXX, XXX, XXX−XXX

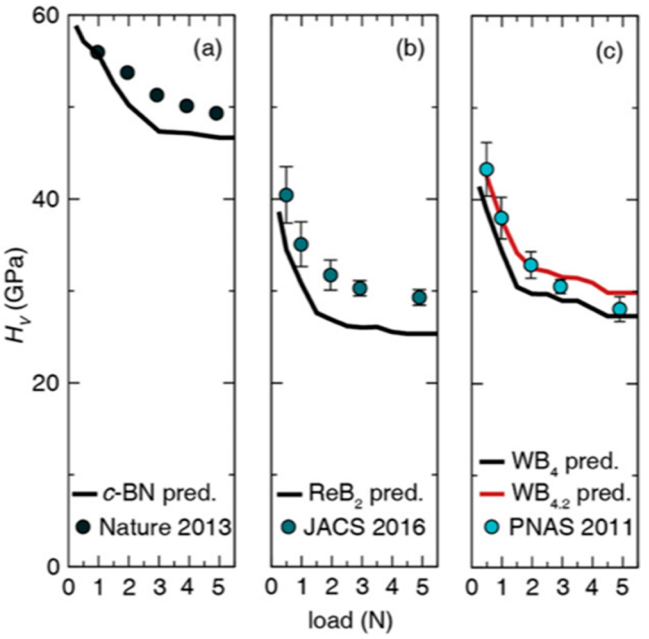

Figure 7. Predictive versus experimentally determined values of load-dependent hardness for (a) c-BN, (b) ReB_2, and (c) WB_4. Reproduced with permission from ref 56. Copyright 2020 John Wiley and Sons.

Since this is a model based solely on composition and does not incorporate crystal structures, certain intrinsic values still need to be manually vetted, such as negative moduli, incompatible crystal types, and hydrogen-incorporated phases.[13] Attempts have been made to search and identify the structures of metal borides through a first-principles global structural optimization method.[57] In addition, new approaches based on the CALYPSO algorithm were used to predict the hardness versus energy map in order to narrow down the energetically favorable superhard materials for syntheses.[58] Although there is still significant progress to be made with these computational tools, machine learning practices that incorporate active learning and neural network-based architectures have proven their value in paving the way for best practices in the field of materials discovery.

5. CONCLUDING REMARKS

Superhard, ultraincompressible materials have been extensively studied over the past decade. Transition metals with high valence electron density combined with small, covalent-bond-forming atoms, such as boron, can be potential candidates for superhard materials. This Account highlights the design of superhard metal borides and discusses the factors that contribute to their high hardness. Furthermore, this work explores future avenues for designing and developing superior materials to meet the needs of next-generation engineering applications.

AUTHOR INFORMATION

Corresponding Authors

Sarah H. Tolbert − *Department of Chemistry and Biochemistry, Department of Materials Science and Engineering, and California NanoSystems Institute (CNSI), University of California, Los Angeles (UCLA), Los Angeles, California 90095, United States;* orcid.org/0000-0001-9969-1582; Email: tolbert@chem.ucla.edu

Richard B. Kaner − *Department of Chemistry and Biochemistry, Department of Materials Science and Engineering, and California NanoSystems Institute (CNSI), University of California, Los Angeles (UCLA), Los Angeles, California 90095, United States;* orcid.org/0000-0003-0345-4924; Email: kaner@chem.ucla.edu

Authors

Lisa E. Pangilinan − *Department of Chemistry and Biochemistry, University of California, Los Angeles (UCLA), Los Angeles, California 90095, United States;* orcid.org/0000-0002-5507-9989

Shanlin Hu − *Department of Chemistry and Biochemistry, University of California, Los Angeles (UCLA), Los Angeles, California 90095, United States;* orcid.org/0000-0002-2288-499X

Spencer G. Hamilton − *Department of Chemistry and Biochemistry, University of California, Los Angeles (UCLA), Los Angeles, California 90095, United States;* orcid.org/0000-0002-0208-1890

Complete contact information is available at: https://pubs.acs.org/10.1021/accountsmr.1c00192

Notes

The authors declare no competing financial interest.

Biographies

Lisa E. Pangilinan obtained a B.S. from Occidental College and a Ph.D. from UCLA. Her Ph.D. research focused on superhard materials.

Shanlin Hu received a B.A. from Boston University and is currently pursuing a Ph.D. at UCLA. Her research focuses on synthesizing nanosuperhard materials and synchrotron-based high-pressure studies.

Spencer G. Hamilton obtained a B.A. from Carleton College and is currently pursing a Ph.D. at UCLA. His research emphasis is on synthesizing superhard materials and synchrotron-based high-pressure studies.

Sarah H. Tolbert obtained a B.A. from Yale University and a Ph.D. from UC Berkeley. She is a Professor in the Departments of Chemistry and Biochemistry and Materials Science and Engineering at UCLA. Research in her group focuses on solution processed nanoscale materials, and on using a combination of nanoscale and atomistic structural control to design new functional materials.

Richard B. Kaner obtained a B.A. from Brown University and a Ph.D. from the University of Pennsylvania. He is a Distinguished Professor in the Departments of Chemistry and Biochemistry and Materials Science and Engineering, and holds the Dr. Myung Ki Hong Endowed Chair in Materials Innovation at UCLA. Research in his group focuses on conducting polymers, superhard materials, and carbon-based compounds.

ACKNOWLEDGMENTS

This work was supported financially by the National Science Foundation Division of Materials Research under grant DMR-2004616 (R.B.K. and S.H.T.). Additional support was provided by the Dr. Myung Ki Hong Endowed Chair in Materials Innovation (R.B.K.), SuperMetalix, Inc. (R.B.K.), and a UCLA Graduate Division Dissertation Year Fellowship (L.E.P.). Data reproduced in this manuscript made use of

beamline 12.2.2 at the Lawrence Berkeley National Laboratory (LBNL). Beamline 12.2.2 at the Advanced Light Source is a DOE Office of Science User Facility supported under contract no. DE-AC02-05CH11231. High pressure research on beamline 12.2.2 is also partially supported by COMPRES, the Consortium for Materials Properties Research in Earth Sciences under NSF Cooperative Agreement EAR 1606856. The authors thank Dr. Abby Kavner, Dr. Reza Mohammadi, and Sabina C. Cabrera for contributing to this work.

REFERENCES

(1) Novikov, N. V.; Dub, S. Fracture Toughness of Diamond Single Crystals. *J. Hard Mater.* **1992**, *2*.
(2) Novikov, N. V.; Dub, S. N.; Mal'nev, V. I. Microhardness and Fracture Toughness of Cubic Boron Nitride Single Crystals. *Sov. J. Superhard Mater.* **1983**, *5*, 16−21.
(3) García, J.; Collado Ciprés, V.; Blomqvist, A.; Kaplan, B. Cemented Carbide Microstructures: A Review. *Int. J. Refract. Hard Met.* **2019**, *80*, 40−68.
(4) Lengauer, W. Transition Metal Carbides, Nitrides, and Carbonitrides. *Handbook of Ceramic Hard Materials*; John Wiley & Sons, Ltd., 2000; pp 202−252.
(5) Yeung, M. T.; Mohammadi, R.; Kaner, R. B. Ultraincompressible, Superhard Materials. *Annu. Rev. Mater. Res.* **2016**, *46*, 465−485.
(6) Occelli, F.; Loubeyre, P.; LeToullec, R. Properties of Diamond under Hydrostatic Pressures up to 140 GPa. *Nat. Mater.* **2003**, *2*, 151−154.
(7) Kenichi, T. Bulk Modulus of Osmium: High-Pressure Powder x-Ray Diffraction Experiments under Quasihydrostatic Conditions. *Phys. Rev. B: Condens. Matter Mater. Phys.* **2004**, *70*, 012101.
(8) Cynn, H.; Klepeis, J. E.; Yoo, C.-S.; Young, D. A. Osmium Has the Lowest Experimentally Determined Compressibility. *Phys. Rev. Lett.* **2002**, *88*, 135701.
(9) Shackelford, J. F.; Alexander, W. *CRC Materials Science and Engineering Handbook*, 3rd ed.; CRC Press: Boca Raton, FL, 2000.
(10) Kaner, R. B.; Gilman, J. J.; Tolbert, S. H. Designing Superhard Materials. *Science* **2005**, *308*, 1268−1269.
(11) Cumberland, R. W.; Weinberger, M. B.; Gilman, J. J.; Clark, S. M.; Tolbert, S. H.; Kaner, R. B. Osmium Diboride, an Ultra-Incompressible, Hard Material. *J. Am. Chem. Soc.* **2005**, *127*, 7264−7265.
(12) Chung, H.-Y.; Yang, J.-M.; Tolbert, S. H.; Kaner, R. B. Anisotropic Mechanical Properties of Ultra-Incompressible, Hard Osmium Diboride. *J. Mater. Res.* **2008**, *23*, 1797−1801.
(13) Pangilinan, L. E.; Hu, S.; Akopov, G.; Cabrera, S. C.; Yeung, M. T.; Mohammadi, R.; Tolbert, S. H.; Kaner, R. B. Superhard Materials: Advances in the Search and Synthesis of New Materials. *Encyclopedia of Inorganic and Bioinorganic Chemistry*; John Wiley & Sons, Ltd., 2021; pp 1−13.
(14) Lei, J.; Hu, S.; Turner, C. L.; Zeng, K.; Yeung, M. T.; Yan, J.; Kaner, R. B.; Tolbert, S. H. Synthesis and High-Pressure Mechanical Properties of Superhard Rhenium/Tungsten Diboride Nanocrystals. *ACS Nano* **2019**, *13*, 10036−10048.
(15) Hume-Rothery, W. *Atomic Theory for Students of Metallurgy*, 5th ed.; The Institute of Metals: London, 1969.
(16) Li, Y.; Bushby, A. J.; Dunstan, D. J. The Hall-Petch Effect as a Manifestation of the General Size Effect. *Proc. R. Soc. London, Ser. A* **2016**, *472*, 20150890.
(17) Akopov, G.; Yeung, M. T.; Kaner, R. B. Rediscovering the Crystal Chemistry of Borides. *Adv. Mater.* **2017**, *29*, 1604506.
(18) Yeung, M. T.; Lei, J.; Mohammadi, R.; Turner, C. L.; Wang, Y.; Tolbert, S. H.; Kaner, R. B. Superhard Monoborides: Hardness Enhancement through Alloying in W1−xTaxB. *Adv. Mater.* **2016**, *28*, 6993−6998.
(19) Pangilinan, L. E.; Turner, C. L.; Akopov, G.; Anderson, M.; Mohammadi, R.; Kaner, R. B. Superhard Tungsten Diboride-Based Solid Solutions. *Inorg. Chem.* **2018**, *57*, 15305−15313.
(20) Lech, A. T.; Turner, C. L.; Lei, J.; Mohammadi, R.; Tolbert, S. H.; Kaner, R. B. Superhard Rhenium/Tungsten Diboride Solid Solutions. *J. Am. Chem. Soc.* **2016**, *138*, 14398−14408.
(21) Mohammadi, R.; Lech, A. T.; Xie, M.; Weaver, B. E.; Yeung, M. T.; Tolbert, S. H.; Kaner, R. B. Tungsten Tetraboride, an Inexpensive Superhard Material. *Proc. Natl. Acad. Sci. U. S. A.* **2011**, *108*, 10958−10962.
(22) Xie, M.; Mohammadi, R.; Turner, C. L.; Kaner, R. B.; Kavner, A.; Tolbert, S. H. Exploring Hardness Enhancement in Superhard Tungsten Tetraboride-Based Solid Solutions Using Radial X-Ray Diffraction. *Appl. Phys. Lett.* **2015**, *107*, 041903.
(23) Akopov, G.; Yeung, M. T.; Turner, C. L.; Mohammadi, R.; Kaner, R. B. Extrinsic Hardening of Superhard Tungsten Tetraboride Alloys with Group 4 Transition Metals. *J. Am. Chem. Soc.* **2016**, *138*, 5714−5721.
(24) Akopov, G.; Yeung, M. T.; Roh, I.; Sobell, Z. C.; Yin, H.; Mak, W. H.; Khan, S. I.; Kaner, R. B. Effects of Dodecaboride-Forming Metals on the Properties of Superhard Tungsten Tetraboride. *Chem. Mater.* **2018**, *30*, 3559−3570.
(25) Akopov, G.; Yeung, M. T.; Sobell, Z. C.; Turner, C. L.; Lin, C.-W.; Kaner, R. B. Superhard Mixed Transition Metal Dodecaborides. *Chem. Mater.* **2016**, *28*, 6605−6612.
(26) Akopov, G.; Roh, I.; Sobell, Z. C.; Yeung, M. T.; Kaner, R. B. Investigation of Ternary Metal Dodecaborides (M1M2M3)B12 (M1, M2 and M3 = Zr, Y, Hf and Gd). *Dalton Trans* **2018**, *47*, 6683−6691.
(27) Akopov, G.; Yeung, M. T.; Turner, C. L.; Li, R. L.; Kaner, R. B. Stabilization of HfB12 in Y1−XHfxB12 under Ambient Pressure. *Inorg. Chem.* **2016**, *55*, 5051−5055.
(28) Chung, H.-Y.; Weinberger, M. B.; Levine, J. B.; Kavner, A.; Yang, J.-M.; Tolbert, S. H.; Kaner, R. B. Synthesis of Ultra-Incompressible Superhard Rhenium Diboride at Ambient Pressure. *Science* **2007**, *316*, 436−439.
(29) Latini, A.; Rau, J. V.; Teghil, R.; Generosi, A.; Albertini, V. R. Superhard Properties of Rhodium and Iridium Boride Films. *ACS Appl. Mater. Interfaces* **2010**, *2*, 581−587.
(30) Lei, J.; Yeung, M. T.; Mohammadi, R.; Turner, C. L.; Yan, J.; Kaner, R. B.; Tolbert, S. H. Understanding the Mechanism of Hardness Enhancement in Tantalum-Substituted Tungsten Monoboride Solid Solutions. *J. Appl. Phys.* **2019**, *125*, 082529.
(31) Yeung, M. T.; Akopov, G.; Lin, C.-W.; King, D. J.; Li, R. L.; Sobell, Z. C.; Mohammadi, R.; Kaner, R. B. Superhard W0.5Ta0.5B Nanowires Prepared at Ambient Pressure. *Appl. Phys. Lett.* **2016**, *109*, 203107.
(32) Akopov, G.; Yin, H.; Roh, I.; Pangilinan, L. E.; Kaner, R. B. Investigation of Hardness of Ternary Borides of the $YCrB_4$, Y_2ReB_6, Y_3ReB_7, and YMo_3B_7 Structural Types. *Chem. Mater.* **2018**, *30*, 6494−6502.
(33) Lech, A. T.; Turner, C. L.; Mohammadi, R.; Tolbert, S. H.; Kaner, R. B. Structure of Superhard Tungsten Tetraboride: A Missing Link between MB2 and MB12 Higher Borides. *Proc. Natl. Acad. Sci. U. S. A.* **2015**, *112*, 3223−3228.
(34) Xie, M.; Mohammadi, R.; Turner, C. L.; Kaner, R. B.; Kavner, A.; Tolbert, S. H. Lattice Stress States of Superhard Tungsten Tetraboride from Radial X-Ray Diffraction under Nonhydrostatic Compression. *Phys. Rev. B: Condens. Matter Mater. Phys.* **2014**, *90*, 104104.
(35) Shumilov, K. D.; Mehmedović, Z.; Yin, H.; Poths, P.; Nuryyeva, S.; Liepuoniute, I.; Jang, C.; Winardi, I.; Alexandrova, A. N. Understanding the Hardness of Doped WB4.2. *J. Phys. Chem. C* **2021**, *125*, 9486−9496.
(36) Akopov, G.; Roh, I.; Sobell, Z. C.; Yeung, M. T.; Pangilinan, L.; Turner, C. L.; Kaner, R. B. Effects of Variable Boron Concentration on the Properties of Superhard Tungsten Tetraboride. *J. Am. Chem. Soc.* **2017**, *139*, 17120−17127.
(37) Lei, J.; Akopov, G.; Yeung, M. T.; Yan, J.; Kaner, R. B.; Tolbert, S. H. Radial X-Ray Diffraction Study of Superhard Early Transition Metal Dodecaborides under High Pressure. *Adv. Funct. Mater.* **2019**, *29*, 1900293.

https://doi.org/10.1021/accountsmr.1c00192
Acc. Mater. Res. XXXX, XXX, XXX−XXX

(38) Mohammadi, R.; Turner, C. L.; Xie, M.; Yeung, M. T.; Lech, A. T.; Tolbert, S. H.; Kaner, R. B. Enhancing the Hardness of Superhard Transition-Metal Borides: Molybdenum-Doped Tungsten Tetraboride. *Chem. Mater.* **2016**, *28*, 632−637.
(39) The Materials Project. Materials Data on YB12 by Materials Project.
(40) Cannon, J. F.; Farnsworth, P. B. High Pressure Syntheses of ThB12 and HfB12. *J. Less-Common Met.* **1983**, *92*, 359−368.
(41) Akopov, G.; Sobell, Z. C.; Yeung, M. T.; Kaner, R. B. Stabilization of LnB12 (Ln = Gd, Sm, Nd, and Pr) in Zr1−XLnxB12 under Ambient Pressure | Inorganic Chemistry. *Inorg. Chem.* **2016**, *55*, 12419−12426.
(42) Komanduri, R.; Shaw, M. C. Wear of Synthetic Diamond When Grinding Ferrous Metals. *Nature* **1975**, *255*, 211−213.
(43) Fahrenholtz, W. G.; Hilmas, G. E. Ultra-High Temperature Ceramics: Materials for Extreme Environments. *Scr. Mater.* **2017**, *129*, 94−99.
(44) Parthasarathy, T. A.; Rapp, R. A.; Opeka, M.; Kerans, R. J. A Model for the Oxidation of ZrB2, HfB2 and TiB2. *Acta Mater.* **2007**, *55*, 5999−6010.
(45) Bsenko, L.; Lundstrom, T. The High-Temperature Hardness of ZrB2 and HfB2. *J. Less-Common Met.* **1974**, *34*, 273−278.
(46) Xiang, H.; Feng, Z.; Li, Z.; Zhou, Y. Temperature-Dependence of Structural and Mechanical Properties of TiB2: A First Principle Investigation. *J. Appl. Phys.* **2015**, *117*, 225902.
(47) Zhang, Z.; Brgoch, J. Determining Temperature-Dependent Vickers Hardness with Machine Learning. *J. Phys. Chem. Lett.* **2021**, *12*, 6760−6766.
(48) Oses, C.; Toher, C.; Curtarolo, S. High-Entropy Ceramics. *Nat. Rev. Mater.* **2020**, *5*, 295−309.
(49) Gild, J.; Zhang, Y.; Harrington, T.; Jiang, S.; Hu, T.; Quinn, M. C.; Mellor, W. M.; Zhou, N.; Vecchio, K.; Luo, J. High-Entropy Metal Diborides: A New Class of High-Entropy Materials and a New Type of Ultrahigh Temperature Ceramics. *Sci. Rep.* **2016**, *6*, 37946.
(50) Feng, L.; Fahrenholtz, W. G.; Hilmas, G. E. Two-Step Synthesis Process for High-Entropy Diboride Powders. *J. Am. Ceram. Soc.* **2020**, *103*, 724−730.
(51) Feng, L.; Fahrenholtz, W. G.; Hilmas, G. E. Processing of Dense High-Entropy Boride Ceramics. *J. Eur. Ceram. Soc.* **2020**, *40*, 3815−3823.
(52) Ma, M.; Ye, B.; Han, Y.; Sun, L.; He, J.; Chu, Y. High-Pressure Sintering of Ultrafine-Grained High-Entropy Diboride Ceramics. *J. Am. Ceram. Soc.* **2020**, *103*, 6655−6658.
(53) Ma, M.; Sun, Y.; Wu, Y.; Zhao, Z.; Ye, L.; Chu, Y. Nanocrystalline High-Entropy Carbide Ceramics with Improved Mechanical Properties. *J. Am. Ceram. Soc.* **2022**, *105*, 606−613.
(54) Feng, L.; Monteverde, F.; Fahrenholtz, W. G.; Hilmas, G. E. Superhard High-Entropy AlB2-Type Diboride Ceramics. *Scr. Mater.* **2021**, *199*, 113855.
(55) Mansouri Tehrani, A.; Oliynyk, A. O.; Parry, M.; Rizvi, Z.; Couper, S.; Lin, F.; Miyagi, L.; Sparks, T. D.; Brgoch, J. Machine Learning Directed Search for Ultraincompressible, Superhard Materials. *J. Am. Chem. Soc.* **2018**, *140*, 9844−9853.
(56) Zhang, Z.; Mansouri Tehrani, A.; Oliynyk, A. O.; Day, B.; Brgoch, J. Finding the Next Superhard Material through Ensemble Learning. *Adv. Mater.* **2021**, *33*, 2005112.
(57) Li, Q.; Zhou, D.; Zheng, W.; Ma, Y.; Chen, C. Global Structural Optimization of Tungsten Borides. *Phys. Rev. Lett.* **2013**, *110*, 136403.
(58) Zhang, X.; Wang, Y.; Lv, J.; Zhu, C.; Li, Q.; Zhang, M.; Li, Q.; Ma, Y. First-Principles Structural Design of Superhard Materials. *J. Chem. Phys.* **2013**, *138*, 114101.

https://doi.org/10.1021/accountsmr.1c00192
Acc. Mater. Res. XXXX, XXX, XXX−XXX